PCCP

Accepted Manuscript

ROYAL SOCIETY OF CHEMISTRY

www.rsc.org/pccp

Chemical Bondings-Induced Rich Electronic Properties of Oxygen Adsorbed Few-layer Graphenes

Ngoc Thanh Thuy Tran,[a] Shih-Yang Lin,*[a] Yu-Tsung Lin,[a] Ming-Fa Lin,[a‡]

Received Xth XXXXXXXXXX 20XX, Accepted Xth XXXXXXXXX 20XX
First published on the web Xth XXXXXXXXXX 200X
DOI: 10.1039/b000000x

Electronic properties of graphene oxides enriched by strong chemical bondings are investigated using first-principles calculations. They are very sensitive to the changes in the number of graphene layer, stacking configuration, and distribution of oxygen. The feature-rich electronic structures exhibit the destruction or distortion of the Dirac cone, opening of band gap, anisotropic energy dispersions, O- and (C,O)-dominated energy dispersions, and extra critical points. All of the few-layer graphene oxides are semimetals except for the semiconducting monolayer ones. For the former, the distorted Dirac-cone structures and the O-dominated energy bands near the Fermi level are revealed simultaneously. The orbital-projected density of states (DOS) have many special structures mainly coming from a composite energy band, the parabolic and partially flat ones. The DOS and spatial charge distributions clearly indicate the critical orbital hybridizations in O-O, C-O and C-C bonds, being responsible for the diversified properties.

1 INTRODUCTION

Graphene has been a mainstream material in science and engineering for many years, mainly owing to its remarkable physical, chemical and material properties. Numerous researchers have tried to diversify the essential properties of graphene by using doping,[1–3] stacking configuration,[4,5] layer number,[6,7] electric or/and magnetic fields,[8–10] and mechanical strain.[11,12] Monolayer graphene has a low-energy isotropic Dirac-cone structure, while it is a zero-gap semiconductor because of the vanishing DOS at the Fermi level (E_F=0). On the other hand, all the few-layer graphenes (FLG) are semimetals with small overlaps in valence and conduction bands, in which the low-lying energy bands are significantly affected by the layer number and stacking configuration. Recently, oxygen adsorbed graphene, so-called graphene oxide (GO), has been the focus of attention due to its opening of band gap and other interesting properties.[13–16] It has promised potential applications in a wide variety of areas, including memristor devices,[17] sensors,[18,19] effective radionuclide removal,[20] and supercapacitors.[21–23] This paper seeks to comprehend and contribute to the understanding of the critical orbital hybridizations in O-O, C-O and C-C bonds by investigating how oxygen adsorption, layer number and stacking configuration can enrich the electronic properties of graphene.

The well known method to produce GO is the Hummers method in which a mixture of sodium nitrate, sulphuric acid and potassium permanganate are used in the synthesis process.[24] Recently, other methods have been developed by adding phosphoric acid combined with the sulphuric acid without sodium nitrate, and increasing the amount of potassium permanganate.[25] The oxygen concentration of 70% can be achieved in this modified method.[25] The geometric structure of GO can be examined using nuclear magnetic resonance (NMR),[26–28], X-ray photoelectron spectroscopy (XPS),[29] and scanning transmission electron microscope-energy-dispersive X-ray spectroscopy (STEM-EDS) mapping.[30,31] On the other hand, theoretical studies have shown the dependence of band gap on the concentration and distribution of oxygen atoms in monolayer graphene oxide (MGO).[32,33] The oxygen absoption has converted a part of sp^2 carbon bonds in pristine graphene to sp^3 bonds in GO.[14] It has been reported that the strong hybridization between the $2p_{x,y}$ orbitals of O atoms and the $2p_z$ orbitals of C atoms is responsible for the opening of band gap.[32] However, this work shows that the above-mentioned orbital hybridization is not exact (discussed later in Figs. 4 and 5). The important orbital hybridizations in O-O, C-O and C-C bonds are not fully analyzed, and the oxygen adsorbed FLG system has not been investigated. Therefore, the critical roles of such bondings in determining the essential properties of oxygen adsorbed FLG are worthy of a systematic study.

In this paper, the strong effects of oxygen atoms on the elec-

[0a] *Department of Physics, National Cheng Kung University, 701 Tainan, Taiwan.*
[0‡] E-mail: mflin@mail.ncku.edu.tw

tronic properties of graphene, with different distributions, layers, and stackings, are investigated using first-principles calculations. The calculated results demonstrate that the bond lengths, energy dispersions, band gap, charge distributions, and DOS are sensitive to the changes in oxygen distributions and geometric structures. Specifically, the energy bands exhibit many great features: the destruction or distortion of Dirac cone, opening of band gap, partially flat bands, energy dispersions related to O-O and C-O bonds, and extra critical points. Such features are reflected in the orbital-projected DOS, including the absence and presence of π band peak, the O-dominated special structures near E_F, and the (C,O)-dominated prominent peaks at middle energy. Furthermore, the diverse orbital hybridizations in C-O, O-O, and C-C bonds will be explored through the DOS and spatial charge distributions to explain the dramatic changes in electronic properties. The above-mentioned results can be verified by experimental measurements, such as angle-resolved photoemission spectroscopy (ARPES)[34] and scanning tunneling spectroscopy (STS).[7]

2 COMPUTATIONAL DETAILS

The first-principles calculations on GO are performed based on density functional theory (DFT) using the Vienna Ab initio Simulation Package (VASP).[35,36] The electron-ion interactions are evaluated by the projector augmented wave method,[37] whereas the electron-electron interactions are taken into account by the exchange-correlation function under the generalized gradient approximation of Perdew-Burke-Ernzerhof.[38] A vacuum layer with a thickness of 12 Å is added in a direction perpendicular to the GO plane to avoid interactions between adjacent unit cells. The wave functions are expanded using a plane-wave basis set with a maximum kinetic energy of 500 eV. All atomic coordinates are relaxed until the Hellmann-Feynman force on each atom is less than 0.01 eV/Å. Furthermore, the semiemprical DFT-D2 correction of Grimme is included in the calculations for multilayer graphenes to correctly simulate the van der Waals (vdW) interactions between layers.[39] The total energy is given by $E_{DFT+D} = E_{KS\text{-}DFT} + E_{disp}$, where $E_{KS\text{-}DFT}$ is the self-consistent Kohn-Sham energy and E_{disp} is a semiempirical dispersion correction. The k-point mesh is set as $200\times200\times1$ in geometry optimization, $30\times30\times1$ in band structure, and $250\times250\times1$ in the DOS for the 1×1 unit cell with zigzag structure. An equivalent k-point mesh is set for other cells depending on their size.

3 RESULTS AND DISCUSSION

The atomic structures of oxygen adsorbed monolayer graphene with top view and side view are shown in Fig. 1. Oxygen atoms are adsorbed on the top graphene layer with O/C ratio of 1/2 (50 %) for zigzag (Fig. 1(a)), armchair (Fig. 1(b)), and chiral (Fig. 1(c)) unit cells, in which carbon atoms are arranged along these edge structures, respectively. In comparison with the two latters, the first one has a lower total ground state energy, demonstrating greater stability. This is in agreement with previous studies which have shown that the higher the symmetry of geometric structure, the more stable the system is.[40] However, the difference in total ground state energy among these configurations is only about 7-8 %, indicating that all the distributions are considerably stable. From the top view, oxygen atoms are at the top between two carbon atoms as so-called the bridge-site. We have checked the most stable sites when oxygen is adsorbed on graphene by comparing their total ground state energies. Among the bridge-, hollow- and top-sites, the first is the most stable one and the second is the least stable one, which agrees with previous studies.[3,41]

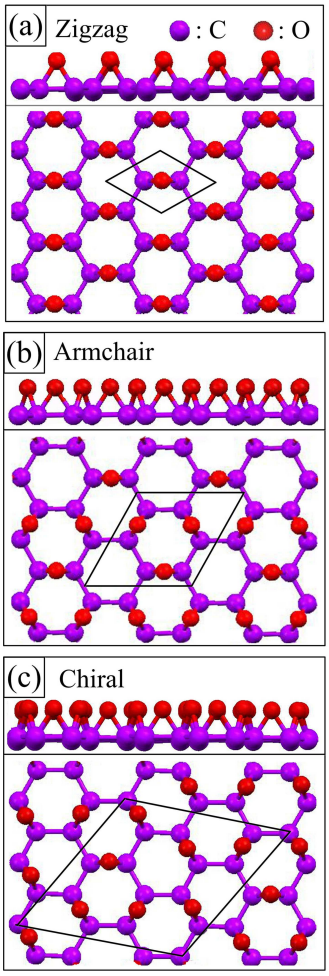

Figure 1 Geometric structures of 50% oxygen concentration systems with: (a) zigzag, (b) armchair, and (c) chiral unit cells.

Table 1 The calculated C-O bond lengths, and C-C bond lengths of the zigzag, armchair, and chiral unit cell with various layers.

Graphene Oxides	C-O bond length (Å)	Nearest C-C bond length (Å)	Second nearest C-C bond length (Å)
Monolayer (zigzag)	1.434	1.503	1.543
Bilayer	1.436	1.459	1.491
Trilayer	1.437	1.441	1.470
Four-layer	1.438	1.432	1.459
Five-layer	1.438	1.431	1.453
Six-layer	1.438	1.430	1.450
Seven-layer	1.438	1.423	1.449
Eight-layer	1.439	1.418	1.444
Nine-layer	1.439	1.416	1.444
Monolayer (armchair)	1.410	1.543	1.569
Bilayer (armchair)	1.413	1.477	1.497
Monolayer (chiral)	1.424	1.519	1.560
Bilayer (chiral)	1.429	1.465	1.496

The main features of geometric structures, including the C-C bond lengths, C-O bond lengths, and interlayer distances are dominated by the number of graphene layer (n). As oxygen atoms are adsorbed on graphene, the C-C bond lengths are expanded compared to 1.424 Å in pristine graphene, as shown in Table 1. The equivalent C-C bond lengths are altered after oxidation, in which the nearest C-C bond corresponding to oxygen atom on the bridge side is shorter than the second nearest one, as a result of the strong C-O bond (Fig. 4(b)). The longer C-C bond length in GO means the $2p_{x,y}$ orbitals of C have the hybridization with atomic orbitals of O. As the layer number grows $n \geq 2$, the C-C bond lengths show a significant decrease while the C-O bond length only has a slight rise. They remain almost unchanged and close to that of pristine graphene for $n \geq 8$. The calculations also reveal that the interlayer distances are affected by oxygen adsorption. The optimized values for AA and AB stackings are equal to 3.27 Å instead of 3.52 Å and 3.26 Å in pristine bilayer systems[5]. Similarly, for AAA and ABA stackings, the interlayer distance between the middle and top layers is about 3.27 Å, whereas that of the bottom and middle layers are nearly identical to the AA- and AB-bilayer ones, respectively. In further examinations, it is found that the n-layer graphene with oxygen adsorbed on the top can be qualitatively regarded as the $(n-1)$-layer of graphene with MGO. The chemical bonding of atomic orbitals will be investigated in more detail later (Fig. 4).

The two-dimensional energy bands along high symmetric points are determined by the C-O, O-O and C-C bonds, oxygen distribution, layer number and stacking configuration (Fig. 2). The contributions of O atoms and C atoms passivated with the former are represented by the blue and red circles, respectively, in which the dominance is proportional to the circle's radius. Different from monolayer graphene, the isotropic Dirac-cone structure near the K point is destroyed in GO, mainly owing to the serious hybridization between the atomic orbitals of C and O atoms (discussed later in charge density and DOS). Such strong C-O bonds lead to the termination of the complete π bonds between parallel $2p_z$ orbitals of C atoms accounting for the Dirac-cone structure near E_F in pristine graphene. Instead, there are wide direct gaps of 3.5 eV, 2.8 eV, and 3.9 eV for the zigzag, armchair, and chiral unit cells, as shown in Figs. 2(a), 2(c) and 2(e), respectively. The highest occupied state is related to an O-dominated energy band. The O-O bond has the weaker σ bond which arises from the $(2p_y-2p_y)$ hybridization for zigzag distribution, and $(2p_{x,y}-2p_{x,y})$ hybridization for armchair and chiral ones (Figs. 4 and 5). As a result, the O-dominated low-lying bands may have the partially flat or parabolic dispersions for the different distributions. On the other hand, the above-mentioned C-O bonds induce the (C,O)-related energy bands at -2 eV$\leq E^v \leq$-4 eV because of the strong orbital hybridizations between passivated C and O atoms (blue and red circles being revealed simultaneously). As to the planar C-C bond, it possesses the strongest σ bond formed by the ($2p_x$, $2p_y$, 2s) orbitals and thus creates the deeper σ bands with $E^v \leq$-3.5 eV (red circles).

For bilayer GO, the band gap is replaced by a distorted Dirac-cone structure that comes from the C atoms on another layer without O passivation. The Dirac point is revealed at the K point for zigzag (Fig. 2(b)) and chiral unit cells (Fig. 2(f)) and at the Γ point for armchair one (Fig. 2(d)). The anisotropic linear bands will change into the parabolic bands with the saddle point along $K \rightarrow M$ or $\Gamma \rightarrow M$. For example, the saddle points of the π and π^* bands, respectively, correspond to $E^v \approx$-2.5 eV and $E^c \approx 1.3$ eV for the zigzag distribution in Fig. 2(b). Different from AA bilayer graphene which has two isotropic Dirac-cone structures with the linear bands intersecting at E_F[5], there is one anisotropic Dirac-cone structure with E_F located at the conduction band. There also exist the O-dominated energy dispersions near E_F and the (C,O)-related bands at middle energy, as revealed in MGO. The band-edge states of the former are above E_F, indicating its free-hole density equal to the free-electron one in the distorted Dirac cone. As the number of graphene layer increases, there are more distorted Dirac cones and saddle points. The band structure differences between AA and AB stackings (Fig. 2(g)) are small and only lie in the crossing and anti-crossing bands (green ellipses). Specially, the energy dispersions of ABA and ABC stackings (Figs. 2(i) and 2(k)) are almost identical, since these two systems correspond to the same structure of AB bilayer graphene with MGO on the top, as proposed ealier in the geometric structures. However, they are different from the AAA stacking in the distorted Dirac-cone structures as well as the crossing and anti-crossing bands (Figs. 2(h) and 2(i)). In addition, the

Fermi velocities of the distorted Dirac cones are reduced about 7−10% compared with that of pristine graphene (≈ 10^6 m/s).[42]

The critical low-energy electronic properties can be further understood by the three-dimensional (3D) bands shown in Fig. 3. The zigzag AA stacking, respectively, exhibits the partially flat and parabolic dispersions on the xz and yz planes (blue and green regions) with the crossing of E_F (Fig. 3(a)). Therefore, the O-dominated energy band can be regarded as a 1D parabolic band. However, this band has the parabolic dispersions (the partially flat dispersions) on the planar projections for the armchair (chiral) distribution, as shown in Fig. 2(c) (Fig. 2(e)). As to the distorted Dirac-cone structures, their main features include the change in energy dispersion, the separation of Dirac points, and the crossing with the O-dominated energy band. For example, the armchair AA stacking possesses an energy spacing of 0.06 eV between two separate Dirac points (near the Γ point in Fig. 3(b)) and one pair of O-dominated parabolic bands at $E^v \simeq$-0.75 eV crossing the valence Dirac cone (Fig. 2(d)). The low-lying energy bands of zigzag AAA and ABA stackings, as shown in Figs. 3(c) and 3(d), clearly illustrate the significant differences in energy dispersions and spacings. The former are two pairs of linear bands with ∼ 0.006 eV energy spacing, whereas the later consist of one pair of parabolic bands and one pair of Mexican-hat bands with ∼ 0.2 eV energy spacing.

Recently, ARPES has emerged as a most useful experimental technique to study the electronic band structures. The experimental measurements on graphene-related systems have been used to investigate the effects due to doping,[43] layer number,[6,44] stacking configuration,[34] and the electric field.[34] For example, they have identified the Dirac-cone structure of graphene grown on SiC,[45] and observed the opening of band gap for graphene on Ir(111) through oxidation.[46] As expected, the feature-rich energy bands of oxygen adsorbed FLG, including the absence and presence of the distorted Dirac-cone structures, the band gap, the O-dominated bands near E_F, and the (C,O)-dominated bands at middle energy can be examined by ARPES. The comparisons between theoretical predictions and experimental measurements can comprehend how oxygen distribution, layer number and stacking configuration affect the electronic properties of oxygen adsorbed FLG.

The charge density (ρ) and the charge density difference (Δρ) can provide very useful information on the spatial charge redistributions and thus on the dramatic changes of energy bands.[47] The former reveals the chemical bondings as well as the charge transfer. In pristine AA stacking (Fig. 4(a)), a strong covalent σ bond with high charge density due to the ($2p_x$,$2p_y$,2s) orbitals exists between two C atoms (the pink rectangle; details in Fig. 4(d)). Furthermore, there is a weak

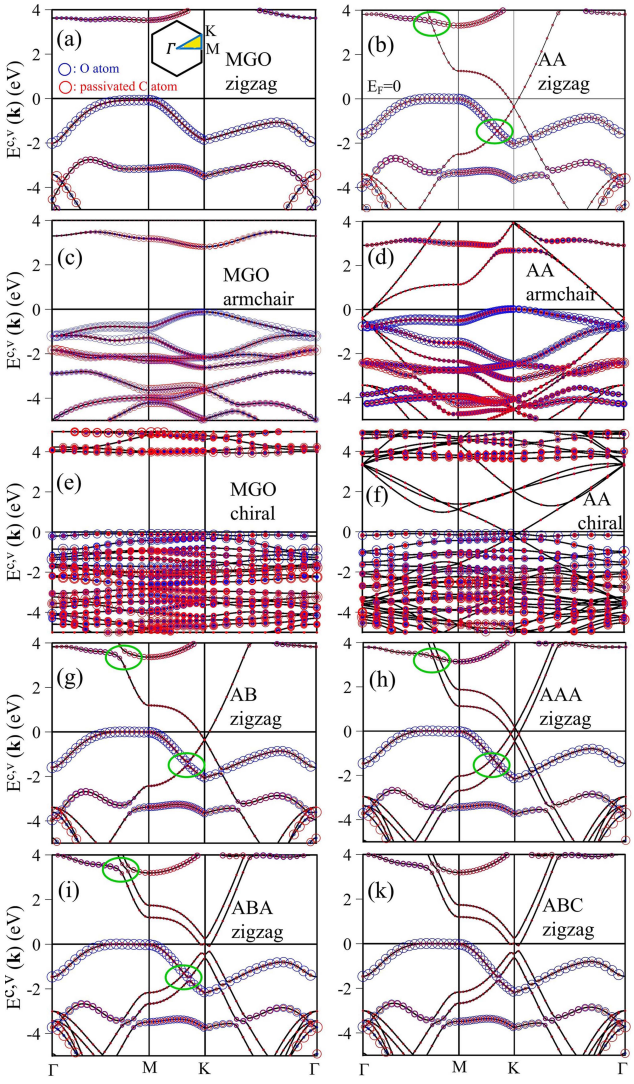

Figure 2 Band structures of the oxygen-adsorbed FLG: (a) monolayer (zigzag), (b) AA bilayer (zigzag), (c) monolayer (armchair), (d) AA bilayer (armchair), (e) monolayer (chiral), (f) AA bilayer (chiral), (g) AB bilayer (zigzag), (h) AAA trilayer (zigzag), (i) ABA trilayer (zigzag), and (k) ABC trilayer (zigzag). Superscripts *c* and *v* correspond to the conduction and valence bands, respectively. Also shown in the inset of (a) is the first Brillouin zone.

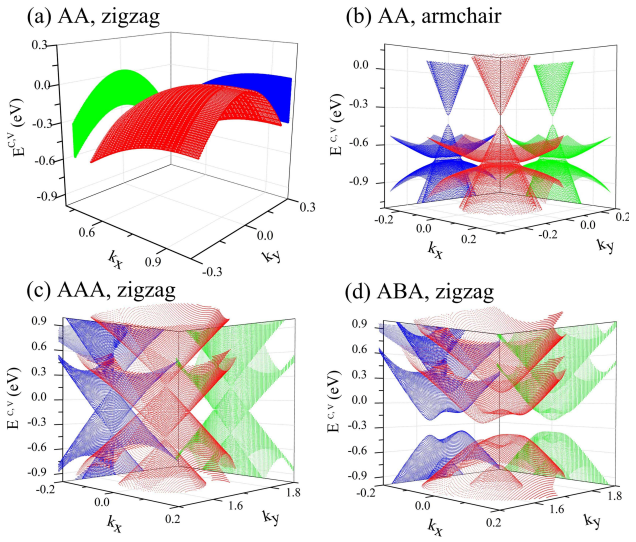

Figure 3 Low-lying 3D band structures for: (a) zigzag AA bilayer near the M point, (b) armchair AA bilayer near the Gamma point, (c) zigzag AAA trilayer near the K point, and (d) zigzag ABA trilayer near the K point.

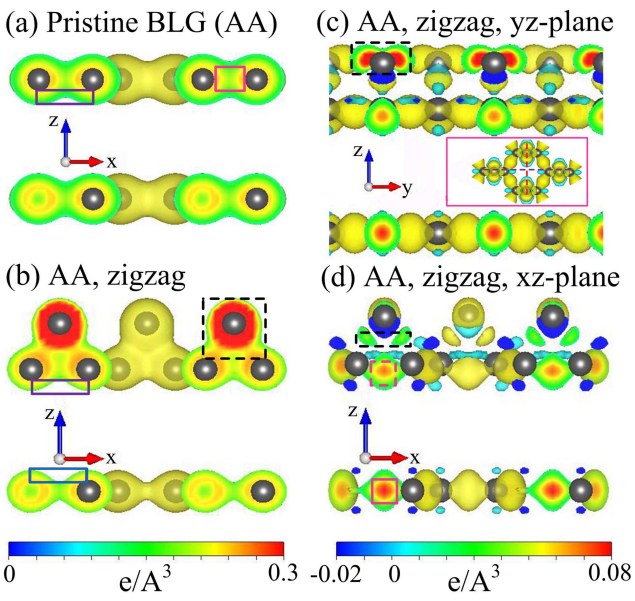

Figure 4 The charge density ρ of (a) pristine AA stacking, and (b) zizag AA bilayer. The charge density difference Δρ of zigzag AA bilayer in (c) yz-plane, and (d) xz-plane.

π bond arising from the parallel $2p_z$ orbitals at the boundary (the purple rectangle). When O atoms are adsorbed on zigzag AA stacking surface (Fig. 4(b)), charges transferred from C to O atoms are $\sim 1e$ using the Bader charge analysis (the dashed black square). The strong C-O bond induces the termination of π bond on the upper boundary and the charge redistribution of π bond on another one. The former accounts for the absence of Dirac cone and the opening of energy gap. The latter is further reflected in the π bond of the bottom layer by the vdW interactions, so that the Dirac cone presents the distorted structure (Fig. 2(b)). The above-mentioned characteristics about the σ and π bonds as well as the strong C-O bond are also found in armchair and chiral distributions.

In order to comprehend the orbital hybridizations in O-O, C-O and C-C bonds, the variation of charge density Δρ of zigzag AA bilayer is illustrated in Figs. 4(c) and 4(d). It is created by substracting the charge density of isolated C and O atoms from that of GO system. The top view of charge density difference of zigzag AA stacking is shown in the inset of Fig. 4(c), where the red and purple dashed lines represent the slices in yz and xz planes, respectively. The p_y orbitals of O with high charge density enclosed in the dashed black rectangle (Fig. 4(c)) are lengthened along $\hat{y}$ compared to isolated O atom's, clearly indicating the $2p_y-2p_y$ hybridization (viewed along the red line of the inset). The O-O bond belongs to a weak σ bond because of the larger distance, being the main reason for the low-lying O-related bands near E_F (Fig. 2(b)). It has also been observed that the O-O bond comes from the hybridization of $2p_{x,y}-2p_{x,y}$ for the armchair and chiral distributions (not shown; Figs. 5(c) and 5(e)). In sharp contrast to the $2p_y$ orbitals, the $2p_z$ and $2p_x$ orbitals of O have strong hybridizations with those of C, as seen from the green region enclosed by the dashed purple rectangle (Fig. 4(d)). This region lies between O and passivated C atoms and bents toward the latter, while the p_y orbitals do not reveal any hybridization with other orbitals. In fact, it is hard to completely distinguish which orbitals have hybridizations to each other by using charge density analysis, but they also show the significant evidences in the orbital-projected DOS (Fig. 5). The C-O bond is much stronger than the O-O bond; therefore, the (C,O)-related bands appear at the range of -2 eV $\leq E^v \leq$ -4 eV. On the other hand, between two non-passivated C atoms of GO, Δρ shows a strong σ bond indicated by the enclosed pink square in Fig. 4(d). Such bond becomes a bit weaker after the C-O bond is formed (the dashed pink square in Fig. 4(d)). This demonstrates that not only the $2p_z$ orbitals of passivated C atoms hybridize with orbitals of O atoms but also the $2p_{x,y}$ orbitals play an important role. However, the planar C-C bond remains the strongest one and has the deeper σ energy bands.

The main characteristics of band structures are directly reflected in DOS. The orbital-projected DOS, as shown in Fig. 5, is useful in understanding the orbital contributions as well as the orbital hybridizations in chemical bonds. The feature-rich DOS presents three kinds of special structures, including the asymmetric peak (circle), the shoulder structures,

and the symmetric peaks. They, respectively, correspond to a composite band with the partially flat and parabolic dispersions, the minimum/maximum band-edge states of parabolic bands, and the saddle points of parabolic bands or the partially flat bands[11]. The low-energy DOS is thoroughly altered after oxygen adsorption. For pristine graphene, the peaks caused by π and π* bands due to $2p_z-2p_z$ bondings between C atoms will dominate within the range of $|E| \leq 2$ eV[42]. However, the π- and π*-peaks are absent as a result of the strong C-O bond. Instead, there are several O-dominated prominent structures in a wide range of $E \sim$-2.5 eV to E_F, mainly coming from the $2p_y-2p_y$ bondings in zigzag distribution (Fig. 5(a)) and the $2p_{x,y}-2p_{x,y}$ bondings in armchair and chiral ones (Figs. 5(c) and 5(e)). It is noticed that the contributions of $2p_x$ and $2p_y$ orbitals in armchair distribution are equivalent because of the symmetric distribution of O atoms. With the addition of graphene layer, the π- and π*-peaks related to the non-passivated C atoms appear around -2.5 eV and 1.2 eV, respectively (arrows in Figs. 5(b), 5(d); 5(f)-5(h)). Apparently, the number of these peaks are only affected by graphene layer number (Figs. 5(b), 5(g) and 5(h)).

With the increasing energy, DOS grows quickly and exhibit prominent symmetric peaks due to the C-O bond at middle energy (-2 eV$\leq E^v \leq$-4 eV). Among these peaks, the most pronounced one is mainly contributed by the ($2p_z$,$2p_x$), ($2p_x$,$2p_y$,$2p_z$) and ($2p_x$,$2p_y$,$2p_z$) orbitals of C and O atoms for the zigzag, armchair and chiral distributions, respectively (e.g., triangles in Figs. 5(a), 5(c); 5(e)). The contributions of distinct orbitals revealed at the same energy apparently represent the significant hybridizations between them, being consistent with those in the spatial charge distributions (Fig. 4(d)). This strong covalent C-O bond is the main reason for the absence of π and π* peaks and the opening of band gap. Also, the magnitude of energy gap depends on the O-O bond strength, as indicated from distinct gaps among three types of distributions.

Up to now, there have been several theoretical studies on GO, especially in electronic properties.[14,32,33,48] They are focused on how the band gap is modulated with the variation of oxygen concentration.[32,33] The orbital hybridizations that cause the opening of band gap and critical electronic properties have not been fully explored. In this work, the comprehensive orbital hybridizations in C-O, O-O, and C-C bonds are analyzed by the spatial charge distributions and orbital-projected DOS (Figs. 4 and 5). The previous study[32] proposed $2p_z-2p_{x,y}$ orbital hybridizations of C and O atoms to explain the opening of band gap, in which they are not totally exact. Our results indicate orbital hybridizations of $2p_{x,z}-2p_{x,z}$ or $2p_{x,y,z}-2p_{x,y,z}$ between passivated C and O atoms, obviously including the $2p_z-2p_z$ hybridizations. The effect of oxygen distributions on the magnitude of band gap has

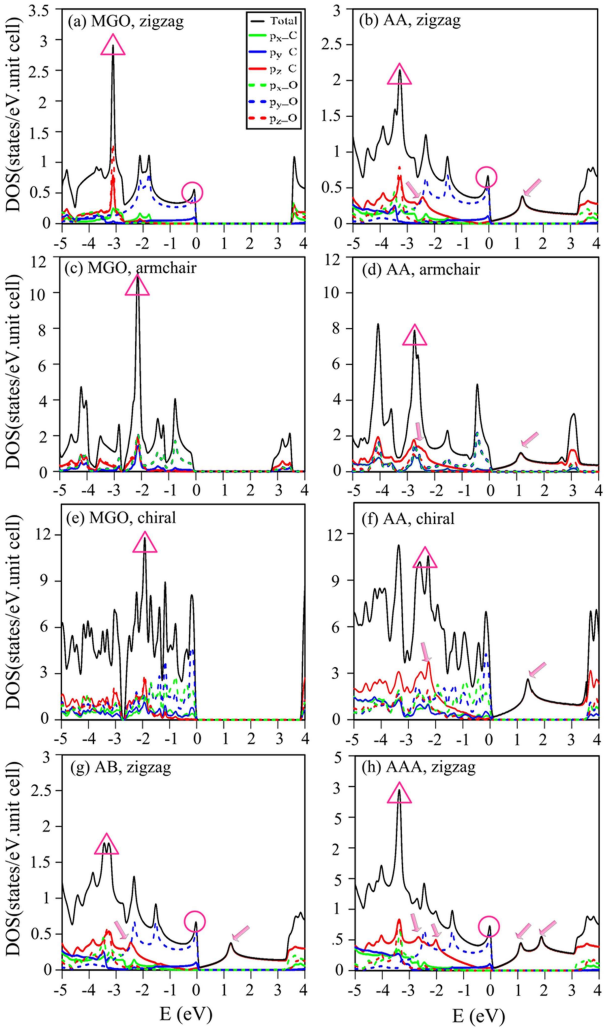

Figure 5 DOS of the oxygen-adsorbed FLG: (a) zigzag monolayer, (b) zigzag AA bilayer, (c) armchair monolayer, (d) armchair AA bilayer, (e) chiral monolayer, (f) chiral AA bilayer, (g) zigzag AB bilayer, and (h) zigzag AAA trilayer.

been pointed out,[14,32] but not the chemical picture for this, the $2p_y-2p_y$ or $2p_{x,y}-2p_{x,y}$ hybridizations in O-O bond. Moreover, the terminated π bond, and the reformed π and σ bonds are clearly illustrated using spatial charge distributions (Fig. 4).

The STS measurements, in which the tunneling conductance (dI/dV) is approximately proportional to DOS and directly reflects its special structures, can provide an efficient way to confirm the distribution of oxygen. This method has been used to investigate the adatom-induced features in monolayer graphene,[49,50] FLG,[7,51] graphene nanoribbons,[52,53] and carbon nanotubes,[54,55] e.g., the observations of the Fermi-level shift and additional peaks near the Dirac point of graphene irradiated with Ar^+ ions.[50] The main features in electronic properties, including the energy gaps, the O-dominated prominent structures near E_F, the high π- and π*-peaks, and the strong (C,O)-related peaks at middle energy, can be further investigated with STS. The STS measurements on the low- and middle-energy peaks can identify the complex chemical bondings in oxygen adsorbed FLG.

In addition, electronic properties are also affected by the both-side adsorption and oxygen concentration, as shown in Fig. S1. Adsorption energy E_{ad} and binding energy E_b in Table S1 indicate that the stabilities are enhanced by the higher oxygen concentration and distribution symmetry. Furthermore, the both-side adsorbed systems are more stable compared to the single-side ones. The former possess smaller band gaps, mainly owing to the weakened interactions between O atoms (see O-O interaction energy in Table S1). For the high O-concentration (50% in Fig. S1(b)), the O-O bonds dominate the lower-energy electronic properties (blue circles), and the Dirac-cone structure arising from the π bonds is absent. With the decrease of O-concentration, the competition between the weakened O-O bonds and the gradually recovered π bonds (from non-passivated C atoms) will lead to the reduced band gap (33% in Figs. S1(c) and S1(d), Table S1). Moreover, the distorted Dirac-cone structure is reformed at the lower concentration, e.g., 25% in Figs. S1(e) and S1(f). The both-side absorbed bilayer graphene can be considered as the superposition of two MGOs. The band structures of AA (Fig. S1(g)) and AB systems are almost the same, revealing the semiconducting behavior. In case of trilayer, the energy dispersions of both-side absorbed AAA, ABA and ABC stackings are almost identical, since they correspond to the same sandwich structure with monolayer graphene at the middle and two MGOs on its top and bottom. There exists a metallic Dirac-cone structure coming from the C atoms of the middle layer without passivation (Fig. S1(h)). The critical orbital hybridizations in O-O, C-O and C-C bonds of both-side adsorbed systems remain similar to the single-side adsorption ones (further see the plotted charge density and charge density difference in Fig. S2). The terminated π bonds and the reformed π bonds are clearly illustrated in the purple rectangles of Figs. S2(a) and S2(b). The former and the latter are responsible for the O-dominated energy bands and the distorted Dirac-done structure, respectively. The strong covalent σ bonds with high charge density exist between two non-passivated C atoms and become weaker when the C atoms are bonded with O atoms (white squares in Figs. S2(c) and S2(d)). A lot of distinct adsorption structures and oxygen concentrations could be further taken into account, and this problem is under current investigation.

4 CONCLUDING REMARKS

The geometric structures and electronic properties of oxygen adsorbed FLG are studied using first-principles calculations. They are shown to be dominated by the diverse orbital hybridizations in chemical bonds. The C-C bond lengths are expanded due to oxygen adsorption and gradually recover to that in pristine graphene with the increasing layer number. The nearest C-C bond length is shorter compared to the second nearest one, indicating the significant interactions between the passivated C atoms and O atoms. The C-C, C-O and O-O bonds are responsible for the dramatic changes in electronic properties, including the destruction or distortion of Dirac cone, energy gap, anisotropic energy spectra, (C,O)- and O-dominated energy bands, and many extra critical points. The oxygen adsorbed FLG, with the O-related energy bands and the distorted Dirac cone near E_F, are semi-metals except for the semiconducting monolayer ones. The predicted feature-rich band structures, which depend on the oxygen distribution, stacking configuration and layer number, could be examined by the ARPES measurements.

The competition or cooperation among the critical chemical bondings in C-C, O-O and C-O bonds can enrich the essential properties. The complete π bondings due to the parallel $2p_z$ orbitals in C-C bonds can be formed on the graphene planes without oxygen adsorption. They are affected by the oxygen passivation so that the distorted Dirac-cone structures exhibit the crossing with the O-dominated band, the energy spacings between the separated Dirac points, and the changes in energy dispersions. Such structures are sensitive to the number of layers and stacking configuration, e.g., the same bands between ABA and ABC stackings, but the distinct bands for ABA and AAA stackings. In addition, the ($2p_x$,$2p_y$,2s) orbitals of C atoms only create the σ bands with the deeper state energies lower than -3.5 eV. The $2p_y-2p_y$ or $2p_{x,y}-2p_{x,y}$ orbital hybridizations in the O-O bonds are determined by the oxygen distribution; furthermore, the sufficiently strong bondings will generate the O-dominated energy dispersions with a bandwidth of $\sim$2.5 eV near E_F. There exist serious orbital hybridizations

of $2p_{x,z}-2p_{x,z}$ or $2p_{x,y,z}-2p_{x,y,z}$ between passivated C and O atoms, thus, leading to the deeper (C,O)-related energy bands at -2 eV$\leq E^{v} \leq$-4 eV, and the absence of the isotropic Dirac cone. This was not clearly explored in the previous studies. [14,32] The main features of the orbital-dependent energy bands are directly reflected in DOS with a lot of peaks and shoulder structures. The experimental examinations of STS on DOS, as well as those of ARPES on energy bands, can provide the full information to understand the complex orbital bondings in GO.

ACKNOWLEDGMENTS

This work was supported by the Physics Division, National Center for Theoretical Sciences (South), the Nation Science Council of Taiwan (Grant No. NSC 102-2112-M-006-007-MY3). We also thank the National Center for High-performance Computing (NCHC) for computer facilities.

References

[1] H. Liu, Y. Liu and D. Zhu, *J. Mater. Chem.*, 2011, **21**, 3335–3345.

[2] D. Wei, Y. Liu, Y. Wang, H. Zhang, L. Huang and G. Yu, *Nano Lett.*, 2009, **9**, 1752–1758.

[3] K. Nakada and A. Ishii, *Solid State Commun.*, 2011, **151**, 13–16.

[4] X. Zhong, R. Pandey and S. P. Karna, *Carbon*, 2012, **50**, 784–790.

[5] N. T. T. Tran, S. Y. Lin, O. E. Glukhova and M. F. Lin, *J. Phys. Chem. C*, 2015.

[6] P. Sutter, M. S. Hybertsen, J. T. Sadowski and E. Sutter, *Nano Lett.*, 2009, **9**, 2654–2660.

[7] P. Lauffer, K. Emtsev, R. Graupner, T. Seyller, L. Ley, S. Reshanov and H. Weber, *Phys. Rev. B*, 2008, **77**, 155426.

[8] Y. K. Huang, S. C. Chen, Y. H. Ho, C. Y. Lin and M. F. Lin, *Sci. Rep.*, 2014, **4**, year.

[9] C. L. Lu, C. P. Chang, Y. C. Huang, R. B. Chen and M. F. Lin, *Phys. Rev. B*, 2006, **73**, 144427.

[10] K. Tang, R. Qin, J. Zhou, H. Qu, J. Zheng, R. Fei, H. Li, Q. Zheng, Z. Gao and J. Lu, *J. Phys. Chem. C*, 2011, **115**, 9458–9464.

[11] J. H. Wong, B. R. Wu and M. F. Lin, *J. Phys. Chem. C*, 2012, **116**, 8271–8277.

[12] V. M. Pereira and A. H. C. Neto, *Phys. Rev. Lett.*, 2009, **103**, 046801.

[13] D. A. Dikin, S. Stankovich, E. J. Zimney, R. D. Piner, G. H. Dommett, G. Evmenenko, S. T. Nguyen and R. S. Ruoff, *Nature*, 2007, **448**, 457–460.

[14] K. A. Mkhoyan, A. W. Contryman, J. Silcox, D. A. Stewart, G. Eda, C. Mattevi, S. Miller and M. Chhowalla, *Nano Lett.*, 2009, **9**, 1058–1063.

[15] M. Hirata, T. Gotou, S. Horiuchi, M. Fujiwara and M. Ohba, *Carbon*, 2004, **42**, 2929–2937.

[16] D. Yang, A. Velamakanni, G. Bozoklu, S. Park, M. Stoller, R. D. Piner, S. Stankovich, I. Jung, D. A. Field, C. A. Ventrice *et al.*, *Carbon*, 2009, **47**, 145–152.

[17] S. Porro, E. Accornero, C. F. Pirri and C. Ricciardi, *Carbon*, 2015, **85**, 383–396.

[18] M. Veerapandian, M. H. Lee, K. Krishnamoorthy and K. Yun, *Carbon*, 2012, **50**, 4228–4238.

[19] J. T. Robinson, F. K. Perkins, E. S. Snow, Z. Wei and P. E. Sheehan, *Nano Lett.*, 2008, **8**, 3137–3140.

[20] A. Y. Romanchuk, A. S. Slesarev, S. N. Kalmykov, D. V. Kosynkin and J. M. Tour, *Phys. Chem. Chem. Phys.*, 2013, **15**, 2321–2327.

[21] Y. Xue, L. Zhu, H. Chen, J. Qu and L. Dai, *Carbon*, 2015, **92**, 305–310.

[22] Y. Chen, X. Zhang, D. Zhang, P. Yu and Y. Ma, *Carbon*, 2011, **49**, 573–580.

[23] W. Gao, N. Singh, L. Song, Z. Liu, A. L. M. Reddy, L. Ci, R. Vajtai, Q. Zhang, B. Wei and P. M. Ajayan, *Nat. Nanotechnol.*, 2011, **6**, 496–500.

[24] W. S. Hummers Jr and R. E. Offeman, *J. Am. Chem. Soc.*, 1958, **80**, 1339–1339.

[25] D. C. Marcano, D. V. Kosynkin, J. M. Berlin, A. Sinitskii, Z. Sun, A. Slesarev, L. B. Alemany, W. Lu and J. M. Tour, *ACS Nano*, 2010, **4**, 4806–4814.

[26] W. Cai, R. D. Piner, F. J. Stadermann, S. Park, M. A. Shaibat, Y. Ishii, D. Yang, A. Velamakanni, S. J. An, M. Stoller *et al.*, *Science*, 2008, **321**, 1815–1817.

[27] C. Hontoria-Lucas, A. Lopez-Peinado, J. d. D. López-González, M. Rojas-Cervantes and R. Martin-Aranda, *Carbon*, 1995, **33**, 1585–1592.

[28] S. Stankovich, D. A. Dikin, R. D. Piner, K. A. Kohlhaas, A. Kleinhammes, Y. Jia, Y. Wu, S. T. Nguyen and R. S. Ruoff, *Carbon*, 2007, **45**, 1558–1565.

[29] W. Gao, L. B. Alemany, L. Ci and P. M. Ajayan, *Nat. Chem.*, 2009, **1**, 403–408.

[30] J. Balamurugan, T. D. Thanh, N. H. Kim and J. H. Lee, *Adv. Mater. Interfaces*, 2015.

[31] X. Zhong, J. Wang, W. Li, X. Liu, Z. Yang, L. Gu and Y. Yu, *RSC Adv.*, 2014, **4**, 58184–58189.

[32] K. Y. Lian, Y. F. Ji, X. F. Li, M. X. Jin, D. J. Ding and Y. Luo, *J. Phys. Chem. C*, 2013, **117**, 6049–6054.

[33] J. Ito, J. Nakamura and A. Natori, *J. Appl. Phys.*, 2008, **103**, 113712.

[34] T. Ohta, A. Bostwick, T. Seyller, K. Horn and E. Rotenberg, *Science*, 2006, **313**, 951–954.

[35] G. Kresse and J. Furthmüller, *Phys. Rev. B*, 1996, **54**, 11169.

[36] G. Kresse and D. Joubert, *Phys. Rev. B*, 1999, **59**, 1758.

[37] P. E. Blöchl, *Phys. Rev. B*, 1994, **50**, 17953.

[38] J. P. Perdew, K. Burke and M. Ernzerhof, *Phys. Rev. Lett.*, 1996, **77**, 3865.

[39] S. Grimme, *J. Comput. Chem.*, 2006, **27**, 1787–1799.

[40] H. Huang, Z. Li, J. She and W. Wang, *J. Appl. Phys.*, 2012, **111**, 054317.

[41] S. Saxena, T. A. Tyson, S. Shukla, E. Negusse, H. Chen and J. Bai, *Appl. Phys. Let.*, 2011, **99**, 013104.

[42] A. C. Neto, F. Guinea, N. Peres, K. S. Novoselov and A. K. Geim, *Rev. Mod. Phys.*, 2009, **81**, 109.

[43] S. Y. Zhou, D. A. Siegel, A. V. Fedorov and A. Lanzara, *Phys. Rev. Lett.*, 2008, **101**, 086402.

[44] T. Ohta, A. Bostwick, J. L. McChesney, T. Seyller, K. Horn and E. Rotenberg, *Phys. Rev. Lett.*, 2007, **98**, 206802.

[45] T. Ohta, F. El Gabaly, A. Bostwick, J. L. McChesney, K. V. Emtsev, A. K. Schmid, T. Seyller, K. Horn and E. Rotenberg, *New J. Phys.*, 2008, **10**, 023034.

[46] K. Schulte, N. Vinogradov, M. L. Ng, N. Mårtensson and A. Preobrajenski, *Appl. Surf. Sci.*, 2013, **267**, 74–76.

[47] S. Y. Lin, S. L. Chang, F. L. Shyu, J. M. Lu and M. F. Lin, *Carbon*, 2015, **86**, 207–216.

[48] D. Sutar, G. Singh and V. D. Botcha, *Appl. Phys. Lett.*, 2012, **101**, 103103.

[49] M. Gyamfi, T. Eelbo, M. Waśniowska and R. Wiesendanger, *Phys. Rev. B*, 2011, **84**, 113403.

[50] L. Tapaszto, G. Dobrik, P. Nemes-Incze, G. Vertesy, P. Lambin and L. P. Biró, *Phys. Rev. B*, 2008, **78**, 233407.

[51] J. Choi, H. Lee and S. Kim, *J. Phys. Chem. C*, 2010, **114**, 13344–13348.

[52] H. Huang, D. Wei, J. Sun, S. L. Wong, Y. P. Feng, A. C. Neto and A. T. S. Wee, *Sci. Rep.*, 2012, **2**, year.

[53] H. Söde, L. Talirz, O. Gröning, C. A. Pignedoli, R. Berger, X. Feng, K. Müllen, R. Fasel and P. Ruffieux, *Phys. Rev. B*, 2015, **91**, 045429.

[54] Y. C. Chen, D. G. De Oteyza, Z. Pedramrazi, C. Chen, F. R. Fischer and M. F. Crommie, *ACS Nano*, 2013, **7**, 6123–6128.

[55] J. W. G. Wilder, L. C. Venema, A. G. Rinzler, R. E. Smalley and C. Dekker, *Nature*, 1998, **391**, 59–62.